Finding the Effective Dynamics to Make Rare Events Typical in Chaotic Maps

Ricardo Gutiérrez[,1,*] Adrián Canella-Ortiz[,2] and Carlos Pérez-Espigares[2,3,†]

[1]*Grupo Interdisciplinar de Sistemas Complejos (GISC), Departamento de Matemáticas, Universidad Carlos III de Madrid, 28911 Leganés, Madrid, Spain*
[2]*Departamento de Electromagnetismo y Física de la Materia, Universidad de Granada, 18071 Granada, Spain*
[3]*Institute Carlos I for Theoretical and Computational Physics, Universidad de Granada, 18071 Granada, Spain*

Dynamical fluctuations or rare events associated with atypical trajectories in chaotic maps due to specific initial conditions can crucially determine their fate, as the may lead to stability islands or regions in phase space otherwise displaying unusual behavior. Yet, finding such initial conditions is a daunting task precisely because of the chaotic nature of the system. In this Letter, we circumvent this problem by proposing a framework for finding an effective topologically conjugate map whose typical trajectories correspond to atypical ones of the original map. This is illustrated by means of examples which focus on counterbalancing the instability of fixed points and periodic orbits, as well as on the characterization of a dynamical phase transition involving the finite-time Lyapunov exponent. The procedure parallels that of the application of the generalized Doob transform in the stochastic dynamics of Markov chains, diffusive processes, and open quantum systems, which in each case results in a new process having the prescribed statistics in its stationary state. This Letter thus brings chaotic maps into the growing family of systems whose rare fluctuations—sustaining prescribed statistics of dynamical observables—can be characterized and controlled by means of a large-deviation formalism.

Introduction.—The study of dynamical large deviations deals with fluctuations of time-averaged observables whose probabilities are exponentially suppressed in time [1–3]. This field has been enriched in recent years by the possibility of constructing effective processes where those rare fluctuations are made typical, i.e., are transformed into high-probability events. This allows for controlling, on demand, the statistics of trajectory observables, which is especially relevant in the context of dynamical phase transitions, allowing, e.g., for the selection of certain dynamical phases that are otherwise extremely unlikely to be observed [4,5]. The methodology combines biased ensembles of time-averaged observables [6,7] with the generalized Doob transform [8–12], and has been recently applied in stochastic systems, including lattice gas models [4,13–15], continuum diffusive systems [11,12,16,17], and many-body systems, both classical [18] and quantum [19–21].

Deterministic dynamical systems are of a different nature, yet they also require a probabilistic description when their evolution is considered from a distribution of initial conditions, which is particularly relevant in the study of chaotic systems [22]. In that respect, the focus of the literature on large deviations of chaotic systems from the last decades of the past century revolves around observables arising in the context of information theory and fractal geometry [23]. A large-deviation approach to chaotic systems based on observables as general as those

considered in stochastic systems, however, seems to have become available only relatively recently. Among those contributions, we highlight the Lyapunov weighted dynamics [24–26], a computational adaptation of the cloning algorithm [27,28] to Hamiltonian systems for selecting trajectories with unusual chaoticity, and the recent extension of the large-deviation formalism to general time-averaged observables in chaotic maps [29]. Despite these advances, the adaptation of the generalized Doob transform, whereby the dynamics creating those rare trajectories is unveiled—thus giving a powerful handle on the analysis and control of large fluctuations—has not yet been accomplished for chaotic maps. This is a conspicuous gap in the literature that we aim to fill with the present work.

In this Letter, we propose a framework for constructing effective maps whose natural invariant measures are tailored to the statistics of general trajectory observables of a given original map. The study of rare events of chaotic maps is thus brought to a level of development that is comparable to that found in recent studies on various types of stochastic systems [4,13,14,18,20]. The goal is illustrated in Fig. 1, which shows an application of our framework to the tent map [23], $x_{n+1} = 1 - |1 - 2x_n|$ [displayed in Fig. 1(a); see Fig. 1(b) for a representative trajectory corresponding to the cobweb plot]. Rare events given by trajectories with an unusually large time spent in a narrow interval centered around the unstable fixed point $x^* = 2/3$ [see Fig. 1(c)], become typical in a new effective
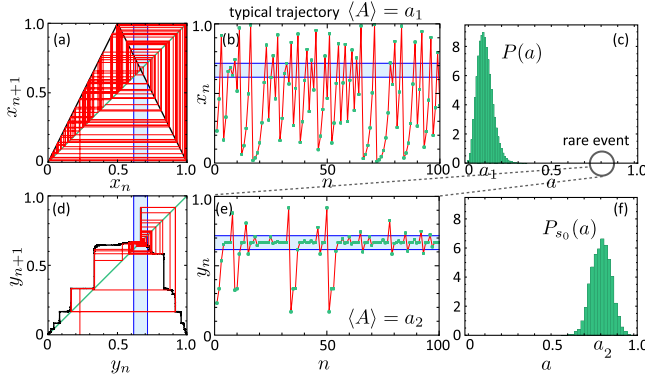
FIG. 1. Rare trajectories due to the repulsive effect of an unstable fixed point are made typical. Fluctuations of the time-averaged indicator function, $A = N^{-1}\sum_{n=0}^{N-1} \mathbb{I}_{[x^*\pm 0.05]}(x_n)$, of the tent map around the unstable fixed point $x^* = 2/3$. (a) Cobweb plot for $N = 100$ iterations. The support of the indicator function is highlighted in light blue. (b) Trajectory illustrated in (a). (c) Histogram, $P(A = a)$, based on 10^5 trajectories, with mean $\langle A \rangle = a_1 = 0.1$. (d) Cobweb plot for $N = 100$ iterations of the Doob effective map with $s_0 = -1$, making typical the rare fluctuation highlighted in (c). (e) Trajectory illustrated in (d). (f) Histogram, $P_{s_0}(A = a)$, based on 10^5 trajectories of the map in (d), with mean $\langle A \rangle = a_2 \approx 0.78$.

map [see Fig. 1(d)], as illustrated in the histogram [Fig. 1(f)] obtained from its trajectories [a representative one is displayed in Fig. 1(e)].

The structure is as follows. We first show how, by extending the generalized Doob transform to the context of Frobenius-Perron operators of chaotic maps, one can generate topologically conjugate effective maps where rare fluctuations of the original dynamics become typical. Then we illustrate our framework by applying it to mitigate the repulsive effect of unstable periodic orbits. Finally, we employ it to characterize dynamical phases involved in a dynamical phase transition associated with the finite-time Lyapunov exponent in the logistic map. Concluding remarks and ideas for future work are presented at the end.

Large-deviation formalism.—We consider a chaotic discrete-time dynamical system $x_{n+1} = f(x_n)$, where $f : I \to I$ is a smooth map and I is some compact interval of the real line. Starting from a probability density of initial values $\alpha_0(x)$, the evolution $\alpha_{n+1}(x) = L[\alpha_n(x)]$ for $n = 0, 1, 2, \ldots$ is given by the Frobenius-Perron operator $L[\alpha(x)] = \int_I \alpha(y)\delta(x - f(y))dy$, where $\delta(x)$ is a Dirac delta [23]. We assume that the map f is ergodic with respect to an invariant measure $\rho(x) = L[\rho(x)]$. The adjoint Frobenius-Perron operator $L^\dagger$ is defined by the equality $\langle \beta, L[\alpha] \rangle = \langle L^\dagger[\beta], \alpha \rangle$, where the angular brackets denote the standard inner product, yielding $L^\dagger[\alpha(x)] = \alpha(f(x))$; see the Supplemental Material (SM) for details [30]. Taking $\beta(x) = \mathbb{1}(x) = 1$ above, it is clear that probability conservation, i.e., $\int L[\alpha(x)]dx = \int \alpha(x)dx = 1$, implies that $L^\dagger[\mathbb{1}(x)] = 1$.

Under quite general conditions, the probability density of the time-averaged observable $A = N^{-1}\sum_{n=0}^{N-1} g(x_n)$ acquires the asymptotic large-deviation form $P(A = a) \sim e^{-NI(a)}$ for long times $N \gg 1$ [32,33]. This probability concentrates around its average value, $\langle A \rangle = \int g(x)\rho(x)dx$, at a rate given by $I(a)$—the so-called rate function—which is non-negative and has a single zero located at $\langle A \rangle$ [2]. Thus fluctuations different from $\langle A \rangle$ become exponentially unlikely in time, and the expansion up to second order of $I(a)$ around the mean displays Gaussian fluctuations with variance $\sigma^2 = [NI''(\langle A \rangle)]^{-1}$. This is illustrated in Fig. 1(c), where the probability of the time-averaged indicator function $A = N^{-1}\sum_{n=0}^{N-1}\mathbb{I}_{[x^*\pm 0.05]}(x_n)$, with $\mathbb{I}_\Omega(x) = 1$ if $x \in \Omega$ and zero otherwise, concentrates around $\langle A \rangle = a_1$.

The conventional method for biasing these probabilities towards specific values of A is to introduce an ensemble of trajectories—known as the s ensemble [1]—such that $P_s(a) = e^{-sNa}P(a)/Z(s)$ with $Z(s) = \int e^{-sNa}P(a)da$. Here s is a biasing field which favors (for $s < 0$) or suppresses (for $s > 0$) the probability of having values larger than $\langle A \rangle$. Thus in Fig. 1 a suitable choice of $s = s_0 = -1$ transforms the probability $P(a)$ with average $a_1 = 0.1$ [Fig. 1(c)], into the probability $P_{s_0}(a)$ with average $a_2 \approx 0.78$ [Fig. 1(f)], which is an unusually large value in the case of the tent map. Indeed, $P(a_2) \sim e^{-NI(a_2)}$ is on the order of 10^{-18} for $N = 100$ [see its position far into the right tail of $P(a)$ in Fig. 1(c)].

In this biased ensemble, the complete statistics of the time-averaged observable A for long times is given by the scaled cumulant-generating function (SCGF) $\theta(s) = \lim_{N\to\infty} N^{-1}\log Z(s)$ [7]. The latter is related to the rate function $I(a)$ by a Legendre transform, $\theta(s) = -\min_a[I(a) + sa]$ [2], highlighting the analogy with the (minus) free-energy and the entropy density in equilibrium statistical mechanics, with the biasing field s playing a role akin to that of the inverse temperature [7]. Since the derivatives of the SCGF provide the cumulants of the observable A in the tilted distribution $P_s(a)$, the (minus) first derivative gives the average $-\theta'(s) = \langle A \rangle_s$. Thus the value of choice for s is the one matching the fluctuation a, such that $-\theta'(s) = a$, or equivalently $I'(a) = s$. In Fig. 1, $-\theta'(s_0) = a_2$ and $I'(a_2) = s_0$, while in the absence of a bias $-\theta'(0) = a_1$ and $I'(a_1) = 0$.

The SCGF is obtained from the spectral problem $L_s[r_s(x)] = e^{\theta(s)}r_s(x)$ [2,29], where $r_s(x)$ is the right eigenfunction associated with the eigenvalue with largest real part, which is $e^{\theta(s)}$, of the so-called tilted Frobenius-Perron operator [30]

$$L_s[\alpha(x)] = \int_I e^{-sg(y)}\alpha(y)\delta(x - f(y))dy$$

$$= \sum_{z \in f^{-1}(x)} \frac{e^{-sg(z)}\alpha(z)}{|f'(z)|}. \tag{1}$$

This is analogous to the definition of a tilted operator for Markov chains [7] and open quantum systems [19], and has been recently studied for chaotic maps [29]. On the other hand, the left eigenfunction of (1), $l_s(x)$, satisfies $L_s^\dagger[l_s(x)] = e^{\theta(s)}l_s(x)$, with $L_s^\dagger$ being the tilted adjoint operator, $L_s^\dagger[\alpha(x)] = e^{-sg(x)}\alpha[f(x)]$, see SM [30]. The eigenfunctions are normalized such that $\int r_s(x)dx = \int l_s(x)r_s(x)dx = 1$. The tilted operator (1), however, does not represent a proper physical evolution, since it does not conserve probability, $L_s^\dagger[\mathbb{1}(x)] \neq 1$. Therefore it is not obvious how to derive a map, associated with L_s, generating the trajectories sustaining the fluctuation a, though such trajectories have been computationally obtained through the Lyapunov weighted dynamics [24]. Our contribution is to show below how to obtain the effective chaotic map [as displayed in Fig. 1(d)] generating those rare trajectories with $s \neq 0$ [see Fig. 1(e)], which follow the biased distribution $P_s(a)$ for long times [Fig. 1(f)]. Such effective dynamics obtained via the Doob transform is in general difficult to construct since one needs to solve the full large-deviation problem. Various numerical schemes, such as the cloning algorithm and transition path sampling complemented with trajectory umbrella sampling [34–36], variational tensor networks [37–39], or machine learning techniques [40,41], have been recently shown to converge to the effective dynamics, but always in the context of stochastic systems.

Doob operator and Doob effective map.—By analogy with the auxiliary Doob process of discrete-time stochastic systems [42,43], we define the Doob operator for a given $s = s_0$, based on the tilted operator (1), its left eigenfunction $l_{s_0}(x)$, and the SCGF $\theta(s_0)$, as

$$L_{s_0}^D[\alpha(x)] = e^{-\theta(s_0)}l_{s_0}(x)L_{s_0}\{[l_{s_0}(x)]^{-1}\alpha(x)\}. \qquad (2)$$

The right eigenfunction associated with the largest eigenvalue of $L_{s_0}^D[\alpha(x)]$, which is 1, is $\rho_{s_0}^D(x) = l_{s_0}(x)r_{s_0}(x)$, and corresponds to the stationary distribution of $L_{s_0}^D$. Indeed, the Doob operator (2) has the two crucial properties we sought: (i) conservation of probability, i.e., $(L_{s_0}^D)^\dagger[\mathbb{1}(x)] = 1$, and (ii) generation of the ensemble of trajectories giving rise to the biased probability $P_{s_0}(a)$ for long times, see SM [30] for details. The atypical fluctuations of the natural dynamics ($s = 0$), associated with some $s_0 \neq 0$ in Eq. (1), thus become typical in the Doob-transformed dynamics (2).

In summary, the Doob operator (2) has a stationary state $\rho_{s_0}^D(x)$ that naturally yields the statistics for A corresponding to rare fluctuations of the original dynamics, which are exponentially suppressed in $\rho(x)$, i.e., the invariant measure of f. Yet we still need the Doob effective map, $f_{s_0}^D$, generating the atypical trajectories $y_{n+1} = f_{s_0}^D(y_n)$, which requires finding a chaotic map with a prescribed invariant measure [44], in this case $\rho_{s_0}^D(y)$. While other maps may have the same invariant measure, the Doob effective map $f_{s_0}^D$ is uniquely defined by the following procedure.

Assuming that $\rho(x)$ and $\rho_{s_0}^D(y)$ are strictly positive and integrable (as in all the examples considered below), so that their cumulative distributions $F(x) = \int_{-\infty}^{x}\rho(u)du$ and $F_{s_0}^D(y) = \int_{-\infty}^{y}\rho_{s_0}^D(u)du$ are continuous and increasing (hence invertible) functions, the transformation that is required is $y = \gamma_{s_0}(x) = (F_{s_0}^D)^{-1}[F(x)]$, as it is easy to verify, see SM [30]. Applying this transformation, it is straightforward to find the Doob effective map taking into account that $y_{n+1} = f_{s_0}^D(y_n) = f_{s_0}^D[\gamma_{s_0}(x_n)]$ and that $y_{n+1} = \gamma_{s_0}(x_{n+1}) = \gamma_{s_0}[f(x_n)]$. From these equations we obtain $f_{s_0}^D[\gamma_{s_0}(x_n)] = \gamma_{s_0}[f(x_n)]$, so that the Doob effective map, which is topologically conjugate to f, takes the form

$$f_{s_0}^D = \gamma_{s_0}\circ f\circ \gamma_{s_0}^{-1}. \qquad (3)$$

The evolution is given by f after a change of coordinates, $y = \gamma_{s_0}(x)$, such that $y_{n+1} = f_{s_0}^D(y_n) = \gamma_{s_0}\{f[\gamma_{s_0}^{-1}(y_n)]\}$. The Doob effective map sustaining the rare event corresponding to $s_0 = -1$ in the example based on the tent map is illustrated in Fig. 1(d); see the SM for the numerical method employed to obtain the eigenfunctions on which its construction is based, where it is illustrated for the doubling map, and compared with analytical and cloning-algorithm results [30]. While a_2 is practically impossible to sample with the original dynamics f, by contrast, in the dynamics given by the effective map $f_{s_0}^D$ it is the average value. Thus the fraction of time spent in the interval $x^* \pm 0.05$ is much higher, 78%, as illustrated in Fig. 1(e), and in the histogram of Fig. 1(f).

Remarkably, while $x^* = 2/3$ is an unstable fixed point of the tent map f, $y^* = \gamma_{s_0}(x^*)$ (which is close to, yet different from, 2/3) is also an unstable fixed point of the Doob map $f_{s_0}^D$. This is true in general and is imposed by the conjugacy: $f_{s_0}^D(y^*) = (\gamma_{s_0}\circ f\circ \gamma_{s_0}^{-1})(y^*) = \gamma_{s_0}[f(x^*)] = \gamma_{s_0}(x^*) = y^*$, and $(f_{s_0}^D)'(y^*) = (\gamma_{s_0}\circ f)'(x^*)(\gamma_{s_0}^{-1})'(y^*) = \gamma_{s_0}'(x^*)f'(x^*)\times[\gamma_{s_0}'(x^*)]^{-1} = f'(x^*)$. Despite this, the peculiar shape of $f_{s_0}^D$ makes the trajectory spend most of the time around x^* [see Fig. 1(d)]. One can similarly show that a fixed point of $f^n = f\circ f\circ\cdots\circ f$ maps into a fixed point of $(f_{s_0}^D)^n$ with the same stability. Those fixed points lie in periodic orbits of f (with period n or integer factors thereof), which is the topic we turn to next.

Counterbalancing the instabilities of periodic orbits.—Unstable periodic orbits are very relevant, as many properties of chaotic systems are analyzed on such orbits embedded within chaotic attractors (see, e.g., Refs. [23,45]). Figure 2 shows how to use our methodology to counterbalance the repulsive effect of unstable periodic orbits. We focus on the logistic map $f(x) = rx(1 - x)$ with $r = 4$ (sometimes called the Ulam map), see the black line in Fig. 2(e). It has a period-two orbit comprising $x_\pm^* = (5 \pm \sqrt{5})/8$, which is unstable, as $(f^2)'(x_\pm^*) = -4$. Because of this instability, the average value of the
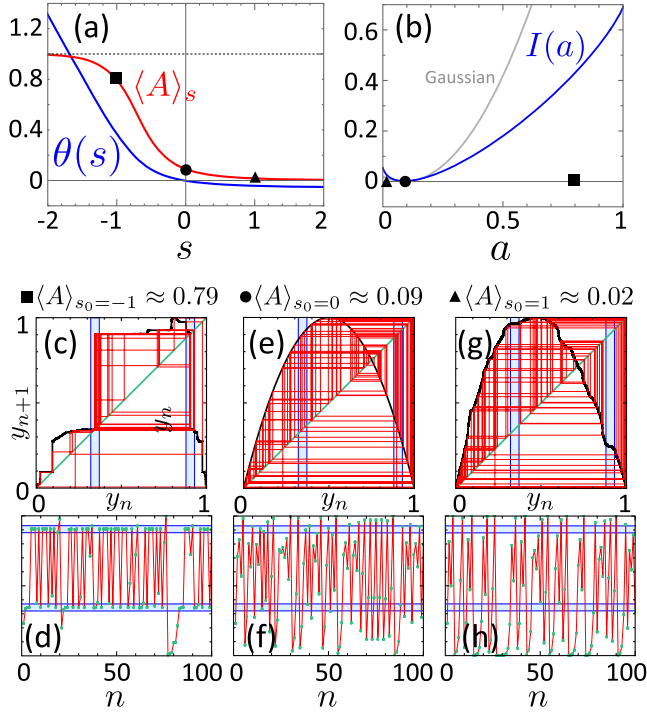
FIG. 2. Rare trajectories due to the repulsive effect of unstable period-two orbits are made typical. Fluctuations of the time-averaged indicator function, $A = N^{-1} \sum_{n=0}^{N-1} [\mathbb{I}_{[x_-^* \pm 0.025]}(x_n) + \mathbb{I}_{[x_+^* \pm 0.025]}(x_n)]$, of the logistic map around the period-two orbit formed by $x_\pm^* = (5 \pm \sqrt{5})/8$. (a) SCGF $\theta(s)$ and biased average $\langle A \rangle_s = -\theta'(s)$. The three points highlighted correspond to $s = -1$ (square), $s = 0$ (circle), $s = 1$ (triangle). (b) Rate function $I(a)$, and Gaussian fluctuations around its average $\langle A \rangle$. (c) Cobweb plot of the Doob effective map for $s_0 = -1$. The support of the indicator function is highlighted in light blue. (d) Trajectory corresponding to the cobweb in (c). (e),(f) Cobweb plot and trajectory of the (unbiased) logistic map ($s_0 = 0$). (g),(h) Cobweb plot and trajectory of the Doob effective map for $s_0 = 1$.

indicator function $A = N^{-1} \sum_{n=0}^{N-1} [\mathbb{I}_{[x_-^* \pm 0.025]}(x_n) + \mathbb{I}_{[x_+^* \pm 0.025]}(x_n)]$ is only $\langle A \rangle \approx 0.09$. See Fig. 2(a), which shows the SCGF $\theta(s)$, as well as its (minus) first derivative $\langle A \rangle_s$, as well as Figs. 2(e) and 2(f), displaying the cobweb plot and a typical trajectory of the unbiased dynamics respectively ($s = 0$). As s is moved towards negative (positive) values, the time average becomes larger (smaller). We will focus on $s_0 = -1$, which yields $\langle A \rangle_{s_0} \approx 0.79$, associated with a much longer time spent in the vicinity of the period-two orbit, and $s_0 = 1$, corresponding to $\langle A \rangle_{s_0} \approx 0.02$, for which the vicinity of the orbit is seldom visited, as displayed by Figs. 2(d) and 2(h), respectively. Those values of s_0 correspond to large deviations of a, well beyond the range of the Gaussian approximation, as shown in Fig. 2(b).

The Doob map for $s_0 = -1$, see Fig. 2(c), is remarkably different from the logistic map, represented in Fig. 2(e). In the case of $s_0 = 1$ [Fig. 2(g)] the difference is more subtle,

yet sufficient for avoiding mapping values of x_n into values of x_{n+1} in the support of the indicator function. The trajectories shown in each case [Figs. 2(d), 2(f), and 2(h)] correspond to the cobweb plots in the panels immediately above, and confirm all expectations.

A dynamical phase transition for the Lyapunov exponent.—To conclude we focus on the timely topic of dynamical phase transitions (DPTs) [7,37,46–51]. Specifically, we characterize the dynamical phases sustaining the fluctuations of the finite-time Lyapunov exponent, $A = N^{-1} \sum_{n=0}^{N-1} \ln |f'(x_n)|$, in the logistic map. For long times, the average of this fluctuating observable, which can be interpreted as a time-averaged information loss [23], converges to the Lyapunov exponent. The latter is $\langle A \rangle = \ln 2$, as obtained from the topological conjugacy of the logistic map and the tent map [23,45]. As the tilting parameter s is varied, one finds that there are just two possible values of the biased average $\langle A \rangle_s$, namely, ln4 and ln2 (including obviously $s = 0$). Indeed the SCGF, which for this observable is closely related to the so-called topological pressure (see, e.g., [23]), is $\theta(s) = -2(s+1) \ln 2$ for $s \leq -2$ and $\theta(s) = -s \ln 2$ for $s \geq -2$, as discussed, with different conventions, in Refs. [52,53] and others therein [54]. Both the SCGF $\theta(s)$ and the average $\langle A \rangle_s = -\theta'(s)$ are displayed in Fig. 3. In this case the rate function is linear, $I(a) = 2(a - \ln 2)$, for $\ln 2 \leq a \leq \ln 4$, and infinite anywhere else.

We next characterize the two dynamical phases, as well as the critical point ($s = s_0 = -2$). For $s < -2$, the Doob effective map, presented on the left of the lower inset to
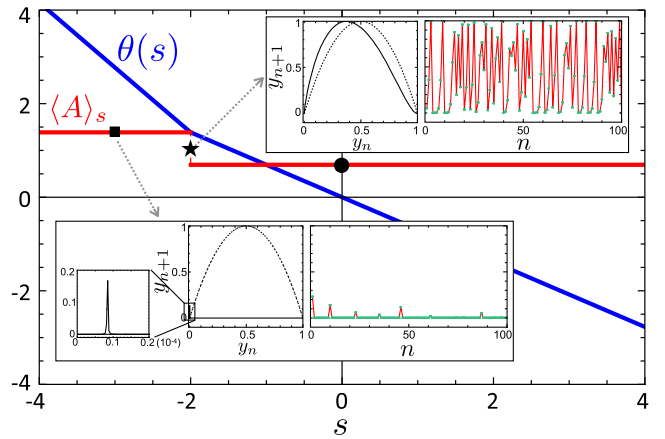

FIG. 3. Characterization of phases in a DPT for the Lyapunov exponent of the logistic map. Main panel: SCGF $\theta(s)$ and biased average $\langle A \rangle_s = -\theta'(s)$. The three points highlighted correspond to $s = -3$ (square), $s = -2$ (star), $s = 0$ (circle). The latter corresponds to the logistic map, shown in Fig. 2(e) with a typical trajectory displayed in Fig. 2(f). Lower inset: Doob effective map and representative trajectory for $s_0 = -3$. Upper inset: same as lower inset but at the critical point $s_0 = -2$, exhibiting coexistence between both dynamical phases. In both insets the original (logistic) map is also shown (see dashed lines).

Fig. 3 for $s_0 = -3$, generates trajectories that localize in the vicinity of the point $x = 0$, as displayed on the right of the same inset. There small intervals expand with a rate ln4 (instead of the common expansion rate ln2 to be found elsewhere in phase space [23,52]), leading to $\langle A \rangle_s = \ln 4$. On the other side of the DPT, for $s > -2$, $\langle A \rangle_s = \ln 2$, as in the unbiased dynamics ($s = 0$), whose trajectories are displayed in Fig. 2(f), where the region around $x \approx 0$ is hardly ever visited. Finally, the Doob effective map at the critical point $s_0 = -2$ is shown in the upper inset to Fig. 3. This map generates trajectories as the one presented on the right of the inset, which exhibits a remarkable intermittency between the behavior for $s_0 = -3$ and for $s_0 = 0$, illustrating the coexistence between dynamical phases characteristic of first-order DPTs [7,17,46,49].

Concluding remarks.—We have developed a theoretical framework to find the effective dynamics realizing atypical trajectories in chaotic maps. Apart from its obvious interest for dynamical control purposes, it allows for the characterization of phases involved in DPTs occurring far away from the unbiased dynamics. While our approach has been developed for 1D systems, the formalism can be extended to cover higher-dimension maps, and perhaps also continuous-time flows. The adaptation of this framework to fluctuations at finite times by means of the finite-time Doob transform may also be feasible with currently available techniques [12,20,38,55].

---

[*] rigutier@math.uc3m.es
[†] carlosperez@ugr.es

[1] J. P. Garrahan, R. L. Jack, V. Lecomte, E. Pitard, K. van Duijvendijk, and F. van Wijland, Dynamical first-order phase transition in kinetically constrained models of glasses, Phys. Rev. Lett. **98**, 195702 (2007).

[2] H. Touchette, The large deviation approach to statistical mechanics, Phys. Rep. **478**, 1 (2009).

[3] R. L. Jack, Ergodicity and large deviations in physical systems with stochastic dynamics, Eur. Phys. J. B **93**, 74 (2020).

[4] R. Hurtado-Gutiérrez, F. Carollo, C. Pérez-Espigares, and P. I. Hurtado, Building continuous time crystals from rare events, Phys. Rev. Lett. **125**, 160601 (2020).

[5] R. Hurtado-Gutiérrez, P. I. Hurtado, and C. Pérez-Espigares, Spectral signatures of symmetry-breaking dynamical phase transitions, Phys. Rev. E **108**, 014107 (2023).

[6] V. Lecomte, C. Appert-Rolland, and F. van Wijland, Thermodynamic formalism for systems with Markov dynamics, J. Stat. Phys. **127**, 51 (2007).

[7] J. P. Garrahan, R. L. Jack, V. Lecomte, E. Pitard, K. van Duijvendijk, and F. van Wijland, First-order dynamical phase transition in models of glasses: An approach based on ensembles of histories, J. Phys. A **42**, 075007 (2009).

[8] D. Simon, Construction of a coordinate Bethe ansatz for the asymmetric simple exclusion process with open boundaries, J. Stat. Mech. (2009) P07017.

[9] V. Popkov, G. M. Schütz, and D. Simon, ASEP on a ring conditioned on enhanced flux, J. Stat. Mech. (2010) P10007.

[10] R. L. Jack and P. Sollich, Large deviations and ensembles of trajectories in stochastic models, Prog. Theor. Phys. Suppl. **184**, 304 (2010).

[11] R. Chetrite and H. Touchette, Nonequilibrium microcanonical and canonical ensembles and their equivalence, Phys. Rev. Lett. **111**, 120601 (2013).

[12] R. Chetrite and H. Touchette, Nonequilibrium Markov processes conditioned on large deviations, Ann. Henri Poincare **16**, 2005 (2015).

[13] R. Gutiérrez and C. Pérez-Espigares, Generalized optimal paths and weight distributions revealed through the large deviations of random walks on networks, Phys. Rev. E **103**, 022319 (2021).

[14] R. Gutiérrez and C. Pérez-Espigares, Dynamical phase transition to localized states in the two-dimensional random walk conditioned on partial currents, Phys. Rev. E **104**, 044134 (2021).

[15] S Marcantoni, C. Pérez-Espigares, and J. P. Garrahan, Symmetry-induced fluctuation relations for dynamical observables irrespective of their behavior under time reversal, Phys. Rev. E **101**, 062142 (2020).

[16] F. Angeletti and H. Touchette, Diffusions conditioned on occupation measures, J. Math. Phys. (N.Y.) **57**, 023303 (2016).

[17] P. Tsobgni Nyawo and H. Touchette, Dynamical phase transition in drifted Brownian motion, Phys. Rev. E **98**, 052103 (2018).

[18] R. L. Jack and P. Sollich, Effective interactions and large deviations in stochastic processes, Eur. Phys. J. Spec. Top. **224**, 2351 (2015).

[19] J. P. Garrahan and I. Lesanovsky, Thermodynamics of quantum jump trajectories, Phys. Rev. Lett. **104**, 160601 (2010).

[20] F. Carollo, J. P. Garrahan, I. Lesanovsky, and C. Pérez-Espigares, Making rare events typical in Markovian open quantum systems, Phys. Rev. A **98**, 010103(R) (2018).

[21] S. Marcantoni, C. Pérez-Espigares, and J. P. Garrahan, Symmetry-induced fluctuation relations in open quantum systems, Phys. Rev. E **104**, 014108 (2021).

[22] J. P. Eckmann and D. Ruelle, Ergodic theory of chaos and strange attractors, Rev. Mod. Phys. **57**, 617 (1985).

[23] C. Beck and F. Schögl, *Thermodynamics of Chaotic Systems: An Introduction* (Cambridge University Press, Cambridge, England, 1993), 10.1017/CBO9780511524585.

[24] J. Tailleur and J. Kurchan, Probing rare physical trajectories with Lyapunov weighted dynamics, Nat. Phys. **3**, 203 (2007).

[25] T. Laffargue, K. Nguyen T. Lam, J. Kurchan, and J. Tailleur, Large deviations of Lyapunov exponents, J. Phys. A **46**, 254002 (2013).

[26] C. Anteneodo, S. Camargo, and R. O. Vallejos, Importance sampling with imperfect cloning for the computation of generalized Lyapunov exponents, Phys. Rev. E **96**, 062209 (2017).

[27] C. Giardinà, J. Kurchan, and L. Peliti, Direct evaluation of large-deviation functions, Phys. Rev. Lett. **96**, 120603 (2006).

[28] C. Giardinà, J. Kurchan, V. Lecomte, and J. Tailleur, Simulating rare events in dynamical processes, J. Stat. Phys. **145**, 787 (2011).

[29] N. R. Smith, Large deviations in chaotic systems: Exact results and dynamical phase transition, Phys. Rev. E **106**, L042202 (2022).

[30] See Supplemental Material at http://link.aps.org/supplemental/10.1103/PhysRevLett.131.227201, which cites Ref. [31], for more detailed discussions about the adjoint operator, the tilted adjoint operator, the Doob effective map, the Doob SCGF, and the numerical method to solve the eigenvalue problem.

[31] B. Derrida and T. Sadhu, Large deviations conditioned on large deviations I: Markov chain and Langevin equation, J. Stat. Phys. **176**, 773 (2019).

[32] Y. Oono and Y. Takahashi, Chaos, external noise and Fredholm theory, Prog. Theor. Phys. **63**, 1804 (1980).

[33] P. Grassberger, R. Badii, and A. Politi, Scaling laws for invariant measures on hyperbolic and nonhyperbolic atractors, J. Stat. Phys. **51**, 135 (1988).

[34] T. Nemoto, F. Bouchet, R. L. Jack, and V. Lecomte, Population dynamics method with a multi-canonical feedback control, Phys. Rev. E **93**, 062123 (2016).

[35] U. Ray, G. K-L. Chan, and D. T. Limmer, Exact fluctuations of nonequilibrium steady states from approximate auxiliary dynamics, Phys. Rev. Lett. **120**, 210602 (2018).

[36] K. Klymko, P. L. Geissler, J. P. Garrahan, and S. Whitelam, Rare behavior of growth processes via umbrella sampling of trajectories, Phys. Rev. E **97**, 032123 (2018).

[37] M. C. Bañuls and J. P. Garrahan, Using matrix product states to study the dynamical large deviations of kinetically constrained models, Phys. Rev. Lett. **123**, 200601 (2019).

[38] L. Causer, M. C. Bañuls, and J. P. Garrahan, Finite time large deviations via matrix product states, Phys. Rev. Lett. **128**, 090605 (2022).

[39] L. Causer, M. C. Bañuls, and J. P. Garrahan, Optimal sampling of dynamical large deviations in two dimensions via tensor networks, Phys. Rev. Lett. **130**, 147401 (2023).

[40] T. Oakes, A. Moss, and J. P. Garrahan, A deep learning functional estimator of optimal dynamics for sampling large deviations, Mach. Learn. **1**, 035004 (2020).

[41] J. Yan, H. Touchette, and G. M. Rotskoff, Learning non-equilibrium control forces to characterize dynamical phase transitions, Phys. Rev. E **105**, 024115 (2022).

[42] C. De Bacco, A. Guggiola, R. Kühn, and P. Paga, Rare events statistics of random walks on networks: Localisation and other dynamical phase transitions, J. Phys. A **49**, 184003 (2016).

[43] F. Coghi, J. Morand, and H. Touchette, Large deviations of random walks on random graphs, Phys. Rev. E **99**, 022137 (2019).

[44] A. Baranovsky and D. Daems, Design of one-dimensional chaotic maps with prescribed statistical properties, Int. J. Bifurcation Chaos Appl. Sci. Eng. **05**, 1585 (1995).

[45] E. Ott, *Chaos in Dynamical Systems*, 2nd ed. (Cambridge University Press, Cambridge, England, 2002), 10.1017/CBO9780511803260.

[46] C. Ates, B. Olmos, J. P. Garrahan, and I. Lesanovsky, Dynamical phases and intermittency of the dissipative quantum Ising model, Phys. Rev. A **85**, 043620 (2012).

[47] R. L. Jack, I. R. Thompson, and P. Sollich, Hyperuniformity and phase separation in biased ensembles of trajectories for diffusive systems, Phys. Rev. Lett. **114**, 060601 (2015).

[48] Y. Baek, Y. Kafri, and V. Lecomte, Dynamical symmetry breaking and phase transitions in driven diffusive systems, Phys. Rev. Lett. **118**, 030604 (2017).

[49] C. Pérez-Espigares, I. Lesanovsky, J. P. Garrahan, and R. Gutiérrez, Glassy dynamics due to a trajectory phase transition in dissipative Rydberg gases, Phys. Rev. A **98**, 021804(R) (2018).

[50] C. Pérez-Espigares and P. I. Hurtado, Sampling rare events across dynamical phase transitions, Chaos **29**, 083106 (2019).

[51] F. Carollo and C. Pérez-Espigares, Entanglement statistics in Markovian open quantum systems: A matter of mutation and selection, Phys. Rev. E **102**, 030104(R) (2020).

[52] T. Tél, Dynamical spectrum and thermodynamic functions of strange sets from an eigenvalue problem, Phys. Rev. A **36**, 2507 (1987).

[53] M. J. Feigenbaum, I. Procaccia, and T. Tél, Scaling properties of multifractals as an eigenvalue problem, Phys. Rev. A **39**, 5359 (1989).

[54] Specifically, $\beta F(\beta)$ in Ref. [52] (which considers a topologically conjugate version of the logistic map) or $G(\beta)$ in Ref. [53] correspond to minus the SCGF, $-\theta(s)$, expressed in terms of the parameter $\beta = s + 1$.

[55] J. P. Garrahan, Classical stochastic dynamics and continuous matrix product states: gauge transformations, conditioned and driven processes, and equivalence of trajectory ensembles, J. Stat. Mech. (2016) 073208.